The maize (*Zea mays* L.) *desynaptic* (*dy*) mutation defines a pathway for meiotic chromosome segregation linking nuclear morphology, telomere distribution, and synapsis.

Shaun P. Murphy[1] and Hank W. Bass[1,2,*]

[1]Institute of Molecular Biophysics, The Florida State University, Tallahassee, FL 32306-4370, USA

[2]Department of Biological Science, The Florida State University, Tallahassee, FL 32306-4295

*Author for correspondence: (bass@bio.fsu.edu)

Running Title: Analysis of the *desynaptic* (*dy*) maize mutant

Key words: Telomeres, Nuclear Envelope, Meiosis

JCS online publication date 2 May 2012

Summary

Meiosis involves a dramatic reorganization of the genetic material along with changes in the architecture of nucleoplasm and cytoplasm. In the opisthokonts, nuclear envelope and meiotic chromosome behavior are known to be coordinated by forces generated in the cytoplasm and transferred to the nucleus by the nuclear-envelope protein linkers SUN and KASH. During meiotic prophase I, the telomere bouquet arrangement is known to play roles in interhomolog recognition, pairing, synapsis, interlock resolution, and homologous chromosome recombination. The maize *desynaptic (dy)* mutant is defective in homologous chromosome synapsis, recombination, telomere–nuclear envelope interactions, and chromosome segregation. A detailed three-dimensional cytological analysis of *dy* revealed telomere misplacement during the bouquet stage, synaptic irregularities, nuclear envelope distortion, and chromosome bridges at anaphase I. Using linkage and B-A translocation mapping, we placed *dy* on the long arm of chromosome 3, genetic bin 3.06. SSR marker analysis narrowed the mapping interval to 9 cM. Candidate genes in this region include a PM3-type SUN domain protein, ZmSUN3. No obvious genetic lesions were found in the *ZmSUN3* allele of *dy*, but a conspicuous splice variant, *ZmSUN3-sv1,* was observed in mRNA from *dy*. The variant message is predicted to result in the synthesis of a truncated ZmSUN3 protein lacking two C-terminal transmembrane domains. Other potential candidate genes relevant to the documented phenotypes were also considered. In summary, this study reveals that *dy* causes disruption of a central meiotic pathway connecting nuclear envelope integrity to telomere localization and synapsis during meiotic prophase.

Introduction

Meiosis is a specialized mechanism by which sexually reproducing species reduce their genomes from diploid to haploid, and the underlying mechanisms are highly conserved among eukaryotes (John, 1990). In general, the process of meiosis is under genetic control and consists of commitment and initiation, homologous chromosome pairing and synapsis, interhomolog reciprocal recombination, disjunctive segregation, and haploid gamete or gametophyte formation. Interhomolog chromosome recombination between parental chromosomes during meiotic prophase I establishes physical connections for bipolar spindle attachment between the homologs, and it generates novel allelic combinations. The study of meiosis in plants has made major contributions to our understanding of this key step in eukaryotic life cycles. See Murphy and Bass (2012) for a review. Telomeres, the structures at the ends of eukaryotic chromosomes, consist of conserved repetitive DNA sequences and associated proteins that regulate genome stability and facilitate meiotic chromosome segregation. During meiotic prophase I, the nucleus is reorganized dramatically—the chromosomes become compact, and their telomeres attach themselves to the surface of the inner nuclear membrane of the nuclear envelope (NE), cluster into a bouquet arrangement, and finally disperse just before NE breakdown at late prophase I but remain attached to the inner nuclear membrane. The formation and dynamics of the bouquet configuration of meiotic chromosomes is thought to contribute to proper homologous chromosome pairing, synapsis, recombination, interlock resolution, and ultimately segregation. For reviews, see Bass (2003), Harper et al. (2004), Scherthan (2007), and Scherthan (2009).

In maize, meiotic telomere clustering occurs *de novo* on the NE during meiotic prophase I, and the spatial and temporal patterns are nearly identical to those in mammals (Bass et al., 1997; Harper et al., 2004; Scherthan, 2009; Scherthan et al., 1996). Telomere-interacting proteins have been identified in fungi and animals and are required for telomere bouquet formation and meiotic chromosome segregation (Chikashige and Hiraoka, 2001; Conrad et al., 2007; Cooper et al., 1998; Ding et al., 2007; Schmitt et al., 2007; Trelles-Sticken et al., 2000). More recently, highly conserved Sad1/Unc-84 (SUN) and KASH (Klarsicht, ANC-1, Syne Homology) domain proteins have been shown to reside at the NE and form a functional bridge required for nuclear migration and anchorage during development and used for meiotic chromosome movements during prophase I. For reviews see Hiraoka and Dernburg (2009), Starr (2009), Starr and Fridolfsson (2010). Proteins with homology to the SUN proteins have recently been described for several plant species (Graumann et al., 2010; Moriguchi et al., 2005; Murphy et al., 2010; Oda and Fukuda, 2011; Van Damme et al., 2004; Zhou et al., 2012), but their function in meiosis remains largely uncharacterized.

Among the model experimental systems for analysis of meiosis, maize is an excellent example and provides one of the best sources of synchronized meiotic cells (Chang and Neuffer, 1989). The meiotic process in higher plants is fairly long (Bennett, 1977) and therefore allows for the collection of multiple developmental time points during meiotic prophase. The ability to observe meiotic chromosomes and nuclear organization within intact nuclei by three-dimensional (3D) optical reconstruction fluorescence microscopy has proven extremely useful in cytological analyses of meiotic mutants. Over 50 meiotic mutants in a variety of maize lines have been identified, many

of them by means of forward genetic screens. For reviews, see Cande et al. (2009) and Golubovskaya et al. (2003). Maize mutants have been classified as those that affect a variety of meiotic events, including meiocyte differentiation, entry into and exit from the meiotic program, sister chromatid cohesion, chromosome condensation, telomere bouquet formation, synapsis, recombination, or those that specifically perturb the meiotic cytoskeleton.

The maize *desynaptic* (*dy*) mutant was initially identified by cytological and genetic approaches as a recessive mutation is manifested in several meiotic defects particularly with respect to chromosome behavior (Nelson and Clary, 1952). The chromosomes in *dy* appear normal at the pachytene stage of male meiotic prophase, but many of the bivalents separate into univalents by late prophase. In previous studies, the chromosomes at the pachytene stage of prophase I appear fully synapsed at first, but they exhibit extensive precocious desynapsis and chiasma-maintenance failure (Maguire et al., 1991; Maguire et al., 1993). Others have shown *dy* to affect the control of meiotic recombination (Ji et al., 1999). 3D telomere FISH analysis of *dy* revealed that the mutation resulted in premature detachment of the telomeres from the NE at pachytene. This defect precedes and probably contributes to the production of chromosome laggards, missegregation, and eventual pollen semisterility (Bass et al., 2003).

Given the multiple meiotic defects attributed to the *dy* mutation, we expected that further investigation would provide insight into the question of whether a SUN-KASH-type complex, known to operate in opisthokont meiosis, is conserved in plants. To examine this question, we undertook a forward genetics approach along with 3D

telomere FISH and immunocytochemistry to characterize *dy.* Here we present evidence that implicates *dy* in connecting the integrity of the NE to telomere behavior and synapsis. Genetic linkage mapping provided an opportunity to examine candidate genes, and information regarding one compelling candidate, *ZmSUN3,* is presented.

Materials and Methods

Plant materials and anther fixation

Maize (*Zea mays* L., 2*n* = 2x = 20) inbred lines (A344+, KYS+, and *dy*) were grown at the Mission Road Research Facility (Tallahassee, FL) greenhouse and summer field plots. Male meiotic cells from meiosis-stage anthers were fixed with formaldehyde in 1× meiocyte buffer A (MBA) as previously described (Bass et al., 1997; Murphy et al., 2010) with either 4% paraformaldehyde, for 3D telomere FISH, or 0.5–1% paraformaldehyde and 0.05% Tween-20, for protein immunolocalization, for 30 min at room temperature. Anthers were then rinsed and stored in MBA for several weeks at 4°C.

Cell staining methods

Cells were prepared for 3D telomere FISH analysis essentially as described by Bass et al. (1997). A fluorescein-conjugated telomere-specific oligonucleotide probe (5'-FITC-$(CCCTAAA)_4$-3') was diluted to 0.13 µM in the hybridization buffer. For immunostaining, fixed anthers were subjected to a 1-hour room-temperature treatment in a triton

permeabilization buffer as previously described (Murphy et al., 2010). The acrylamide pads on the slides were then incubated in blocking buffer containing a 1:250 dilution of primary rabbit polyclonal antibody , α-ASY1 (a gift from F. C. Franklin, University of Birmingham, United Kingdom) then in a FITC-goat anti-rabbit secondary antibody at 1:2,000 in blocking buffer for detection . After staining, cells were counterstained with DAPI at 3 µg/mL in 1× PBS and mounted as previously described (Bass et al., 2003; Bass et al., 1997). Staging of meiotic nuclei was based on chromosome fiber appearance (Bass et al., 2003).

3D imaging, data analysis, and model building

All images were collected with an IX-70 inverted wide-field epifluorescence microscope (Olympus Corporation, Center Valley, PA) with a single oil-immersion lens, 60× (NA 1.4 Plan Apo). Data were sampled in the X, Y, and Z dimensions with voxel dimensions of 0.07 × 0.07 × 0.3 μm^3 and were collected for an area extending ~3–4 µm beyond the nuclear border in Z, and at least 5 µm beyond the edge of the nucleus in X and Y. The resulting data sets were then subjected to 12 cycles of iterative 3D deconvolution before data analysis. Deconvolved images were adjusted by linear scaling for brightness and contrast with SoftWorx (Applied Precision, Issaquah, WA). Telomere position analysis was carried out with 3D modeling and measurement software (SoftWorx). The 3D nuclear shape analysis was carried out on a 0.9 µm projection (3 Z slices) from the middle of the nucleus. Nuclear edges were defined with 2D EditPolygon, and the resulting images were imported into ImageJ (Abramoff et al., 2004) for measurements and analysis. The nuclear circularity (4π[area/perimeter^2]) and aspect ratios were

determined on these polygon circles with tools available in ImageJ. One-way analysis of variance was used to test for differences between the samples analyzed. A Tukey's post-hoc multiple comparison test was used to determine which of the means were statistically different from one another at the 95% confidence level.

DNA isolation and quantification

Approximately 1.5 g of leaf tissue was harvested, flash frozen in liquid nitrogen, and stored at –80°C. DNA was extracted with an aqueous extraction buffer as previously described with some modifications (Dellaporta, 1985). Initially, 9 mL of prewarmed (65°C) extraction buffer (50 mM Tris-HCL, pH8, 10 mM EDTA-NAOH, pH8, 100 mM NaCL, 1% w:v SDS, 1% w:v polyvinylpyrrolidone, and 1% w:v polyvinylpolypyrrolidone) was added to the tissue powder, shaken vigorously for 20 seconds, and incubated at 65°C for 20 minutes. The final DNA pellet was resuspended in 400 µL of TER (10 mM Tris-HCL, pH 8, 0.02 mM EDTA, 40 µg/mL RNAse-A), and the DNA was re-precipitated by the addition of 40 µL 3 M sodium acetate (pH 5.2) and 800 µL of ice-cold ethanol. The DNA was pelleted by centrifugation, washed with 70% ice-cold ethanol, air dried, and resuspended in 250 µL of TER buffer. The resulting DNA yield and quality were assessed by agarose gel electrophoretic analysis, and spectroscopic quantification of the DNA yield was performed with a Nano-drop (Thermo Scientific, ND-1000, Wilmington, DE).

Linkage mapping of maize *desynaptic (dy)*

A monohybrid mapping population was created from genetic crosses between homozygous maize *dy/dy* and inbred line KYS+/+, and the resulting F1 progeny seed were planted and selfed to produce a segregating population. F2 individuals were used for leaf DNA preps and self-fertilized for cytological scoring of F3 meiotic cells. DNA samples were isolated from mutant (*dy/dy*) and nonmutant (+/+ or +/*dy*) and used for bulked-segregant analysis (Michelmore et al., 1991) mapping (Sigma, Maize Mapping SSR primer set, M4193). Upon detection of two consecutive *dy*-linked markers (*p-bnlg1160, p-bnlg197*), additional nearby SSR markers were obtained for finer-resolution mapping (Supplemental Table S1). B-A translocation mapping (Beckett, 1978) was used to confirm the linkage analysis data. B-A translocation stocks (Tb-3La and Tb-3La-2s [6270]) were obtained from the Maize Genetics Cooperation Stock Center. Plants harboring B-A translocations were crossed as male parents to F3 homozygous *dy* plants. Sixteen progeny resulting from these crosses were planted, grown to meiosis stages, and scored cytologically for the *dy* phenotype including chromosome bridges, laggards, and micronuclei.

Bioinformatic screen for candidate genes

Candidate genes were initially identified by inspection of the genome annotations and gene models from the reference genome of B73 (AGPv1 and AGPv2 at http://maizesequence.org and http://maizegdb.org). Specifically, the dy-linked genes within the *dy* mapping interval (*umc1730* at Chr3:171,427,820 to *bnlg1047a* at Chr3:179,119,635) for B73 AGPv2 were examined, and candidates were tabulated if they or BLAST-based homology searches indicated relevance to *dy* phenotypes.

Molecular cloning and RT-PCR of *ZmSUN3*

For genomic and cDNA molecular cloning of *ZmSUN3*, DNA from B73+, KYS+, A344+, and verified *dy/dy* gene-specific primers (see Supplemental Table S2) were designed to span the entire open reading frame, including the 5' and 3' UTR regions. PCR products from the individual reactions were cloned (Topo-TA PCR 2.1, Life Technologies, Grand Island, NY), sequenced, and assembled into a gene structure by means of the contig-assembly software and sequence-analysis program Sequencher v 4.7 (Gene codes Corporation, Ann Arbor, MI). For RT-PCR, total RNA was isolated from meiotic florets microdissected from pre-emerged tassels with the plant RNeasy kit (Qiagen, Valencia, CA). The total RNA was treated with 10 U of RNAse-free DNAse-I (Sigma-Aldrich Corporation, St. Louis, MO) and then reverse transcribed into cDNA with SuperScript III (Life Technologies, Grand Island, NY). Gene-specific primers were designed for *ZmSUN3* on the basis of the cDNA or gene model sequences from the maize genome browser (http://maizesequence.org). RT-PCR products were then resolved, analyzed, cloned, and sequenced as described above.

Results

To begin to investigate the molecular basis of the function of the wild-type *Desynaptic* (*Dy*) gene, we carried out 3D cytological phenotypic analyses using telomere FISH, ASY1 immunolocalization, and nuclear shape analyses. This together

with a forward genetic approach should help to identify the genetic lesion underlying the *dy* mutant phenotypes. First described in 1952, *dy* is a mutant characterized by a partial male semi-sterility phenotype in which bivalent desynapsis leads to univalents by late prophase. Subsequently, others have shown *dy* lines of maize have a defect in chiasma maintenance (Maguire et al., 1991), recombination (Ji et al., 1999), and are prone to telomere-NE interaction defects at mid-prophase (Bass et al., 2003). Given these prior observations, we reasoned that a detailed 3D cytological analysis of *dy* would provide insights into the complex mechanisms that link telomere dynamics to chromosome behavior during meiosis, especially at mid-prophase when synapsis and recombination go to completion.

_dy_ disrupts telomere clustering at the bouquet stage in early meiotic prophase

The effect of the *dy* mutation on telomere localization at the bouquet stage (early meiotic prophase) is shown in Fig. 1. The normal telomere clustering in a wild-type maize zygotene-stage nucleus (A-D) shows more than 90% of the telomere FISH signals are at the nuclear periphery . In a comparable stage in a *dy/dy* nucleus, only ~60–70% of the telomeres are at the nuclear periphery (E-H). These values were typical of the other *dy/dy* nuclei. Nonperipheral telomeres, are those that are located at least 1 µm from the nuclear periphery, are indicated here as by arrows (F) or yellow signal (H). These examples are consistent with our summary observations which were based on visual inspection (n = at least 150 cells), 3D data collection (n = at least 30 cells), and 3D modeling (n = at least 10 cells) of *dy* nuclei at the bouquet-stage. In the case of *dy*, the bouquet stage is defined by telomere clustering, thin fiber appearance,

and eccentric nucleolus. Our finding of a partial bouquet represents the earliest known defect reported for maize *dy*, occurring just before the previously reported telomere-misplacement phenotype of precocious telomere-NE detachment at pachytene (Bass et al., 2003).

_dy_ causes synaptic irregularities at the pachytene stage during mid-prophase

The plant protein ASY1 is localized to the nucleus and associates with chromosome axes at early meiotic prophase (Armstrong et al., 2002; Caryl et al., 2000; Mikhailova et al., 2006). Anti-ASY1 antisera raised against *Arabidopsis* ASY1 have been shown to cross react with those of other plant species, including *Brassica* (Armstrong et al., 2002), rye (Mikhailova et al., 2006), and maize (Golubovskaya et al., 2006; Golubovskaya et al., 2011; Pawlowski et al., 2009; Wang et al., 2009). In maize, ASY1 antiserum produces continuous staining along the length of the meiotic chromosome fibers during early prophase, but the signal becomes undetectable by pachytene, once synapsis is complete (Golubovskaya et al., 2006). The results of the use of this ASY1 antiserum at early and middle prophase are shown in Fig. 2. Distribution of ASY1 along the chromosome fiber axes was normal at zygotene for both wild-type and *dy* nuclei (compare Fig. 2B and 2H), but the patterns at midprophase differed markedly. Wild-type nuclei were unstained at pachytene (Fig. 2E), but ASY1 staining persisted during pachytene in *dy*, indicating incomplete, partial, or disrupted progression of synapsis as shown for a representative nucleus (Fig. 2K). The summary observations presented here are based on visual inspection (n = at least 200 cells) and 3D data collection and analysis (n = at least 50 cells) of nuclei at the pachytene stage of meiosis.

_dy_ causes major nuclear distortion during mid-prophase

Many pachytene-stage nuclei derived from *dy* lines of maize were severely warped and misshapen in appearance. Fig. 3 shows through-focus projections of DAPI-stained pachytene-stage nuclei (*n* = 15) from two wild-type lines (A344+, Fig. 3A–C, and KYS, Fig. 3D–F) and *dy/dy* (Fig. 3G–U). This figure also shows periphery tracings made on a 3-section (0.9 µm) projection from the middle region of the data (grey-filled objects) used for shape analyses. A one-way analysis of variance in conjunction with a Tukey's multiple comparison test revealed that calculated means for the average degrees of circularity for A344 and KYS wild-type nuclei (0.89, SD ± 0.01, and 0.88, SD ± 0.01, respectively) different significantly from that of mutant *dy* pachytene stage nuclei (0.74, SD ± 0.06) (Fig. 3V). A second measure of nuclear shape, the average aspect ratios of best-fit ellipses, for wild-type nuclei 1.16 (A344, SD ± 0.11, and 1.11, KYS; SD ± 0.06) differed than those for *dy* pachytene stage nuclei (1.43m SD ± 0.29; Fig. 3W). This information represents the first report of nuclear deformation for a maize meiotic mutant.

_dy_ causes chromosome bridges, laggards, and micronuclei after meiotic prophase.

The *dy* mutation is known to produce univalents during meiotic prophase, which give rise to micronuclei resulting from chromosome segregation (Nelson and Clary, 1952). At the later stages of meiosis, our observations revealed two phenotypes (laggards and micronuclei) known to result from the univalents produced by the *dy* mutation (Nelson and Clary, 1952), in addition to anaphase chromosome bridges, all of which are shown

in Fig. 4. The anaphase bridges (Fig. 4F) presumably reflect failure of homologous chromosomes to produce normal bivalents and result from unresolved interlocks, recombined dicentric chromosomes, or missegregation of multicentric multivalent figures. The micronuclei may represent intact univalents or chromosome fragments or a combination of the two. Although our results cannot distinguish among these possibilities, the chromosome structures that do not end up at the spindle pole remain as unitary discrete micronuclei in the cytoplasm (Fig. 4H-J, arrows). Of all the phenotypes we have now associated with *dy*—partial bouquet, pachytene telomere internalization, distorted midprophase nuclear shape, irregular ASY1 staining, and chromosome segregation defects detected after meiotic prophase—we find that the last is the simplest and clearest phenotype to obtain, requiring only general chromatin staining techniques and single optical section imaging. For subsequent phenotyping assays associated with linkage mapping of *dy*, we chose the univalent/micronucleus detection assay, as shown in Fig. 4.

Maize *dy* maps to chromosome 3L, genetic bin 3.06

Several desynaptic mutants have been described in maize, but only one, *dsy2*, has been localized to genetic bin 5.04 by B-A translocation and SSR linkage mapping (Franklin et al., 2003). Our similar forward genetic approach, employing bulked segregant analysis (BSA) and B-A translocation mapping (Beckett, 1978; Michelmore et al., 1991) is summarized in Fig. 5. The BSA mapping scheme begins with a cross between *dy* as the male parent and a wild-type female (+/+, KYS). KYS was chosen because it lends itself well to cytology at midprophase. Self-fertilized F1 plants

produced a segregating F2 population. F2 plants were used as leaf source for DNA preparations, and pollen viability assays were attempted but found to be unsatisfactory for unambiguous distinction of mutant (*dy/dy*) from nonmutant (*dy*/+, +/*dy*, or +/+) plants. Instead, we selfed all F2 plants and scored F3 progeny using the univalent/micronucleus-detection assay to determine which F2 plant DNAs were to be pooled for mutants and which for nonmutants. BSA mapping revealed cosegregation of markers on the long arm of chromosome 3. Additional SSR markers (Supplemental Table S1) were obtained in the area of linkage, and cosegregation analysis was carried out on DNA from individual F2 mutants (n = 22) to narrow down the mapping region. In addition, B-A translocation mapping was carried out with stocks that uncover mutants on chromosome 3L (Tb-3La and Tb-3La-2s6270). From progeny analysis of TB-3LA x *dy*, we observed that 7 of 13 progeny from one cross and 3 of 6 progeny from another were cytologically like *dy.* From progeny analysis of TB-3La-2S x *dy*, we observed that 6 of 15 progeny were cytologically like *dy.* Collectively, these observations agree with the expected detection of 50% mutant frequency from B-A translocation test crosses for mutations that reside in the hemizygous region.

The first two markers (*bnlg1160* and *bnlg197*) that showed linkage by BSA mapping are in the chromosomal linkage bin 3.06. Subsequent follow-up mapping with additional SSR loci in the region placed *dy* between *umc1730/zmm16* and *bnlg1047a*, and a total of five markers showed complete linkage to *dy* (Fig. 6C–D). The location of this interval is shown for several maize linkage maps including the reference map, *UMC 1998* (Davis et al., 1999). Markers are shown or estimated for the *dy* mapping interval on the *Genetic 2008 3* and *IBM2 2008 Neighbors 3* maps. The approximate locations of

the B-A translocation stocks are indicated on the basis of extrapolation with the Morgan-to-McClintock translator (Lawrence et al., 2006). Using the univalent/micronuclei scoring assay, we have now mapped *dy* to an ~9-cM region within genetic bin 3.06 on the long arm of chromosome 3.

Identification of *ZmSUN3* as a candidate gene for *dy*

Our exploration of the maize genome for candidate genes in the *dy* mapping interval, in particular, genes that if mutated could result in one or more of the *dy*-associated phenotypes, is summarized in Fig. 7. The genomic region of the *dy* mapping interval (*umc1730* – bnlg1047a) spans 7.7 Mbp and includes 154 gene models, some of which are named, whereas others are unclassified and predicted to encode proteins with unknown function. For this last group, we carried out BLAST homology searches using other databases (www.plantgdb.org; GenBank) to identify proteins or protein domains for our assessments.

Omitting consideration of transposable-element genes, we identified about 20 genes that matched our search criteria. Among these, we found one very compelling candidate gene, a maize SUN-domain protein gene, *ZmSUN3* (Murphy et al., 2010) (Fig. 7C–D). SUN-domain proteins are localized to the inner nuclear membrane of the NE, where they function as part of a physical structure that tethers the cytoplasm to the nucleoplasm, including specific roles in meiotic telomere dynamics during meiotic prophase in animals and fungi (Hiraoka and Dernburg, 2009; Starr and Fridolfsson, 2010). The *ZmSUN3* gene in the maize *dy* mapping region is therefore considered a compelling candidate gene for further examination. It belongs to the recently identified

PM3-type class of SUN-domain proteins, characterized by having a SUN domain in the middle of the protein, 3 trans-membrane domains, a coiled coil domain, and a highly conserved PAD region of unknown function (diagrammed in Fig. 7D). The ESTs that map to this region (Fig. 7C) and gene structure models (Fig. 7D) show the gene intron-exon structure of *ZmSUN3* and the resulting predicted protein and its domains.

Our cloning and sequencing of multiple genomic PCR products and cDNA clones from various genetic sources did not reveal any obvious *dy*-specific genetic lesion in the *SUN3* gene. In particular, we observed several SNPs and a few genotype-specific amino acid variants but did not detect any frameshift, nonsense, or mobile-element insertion in the Zm*SUN3* gene in the *dy* genetic background. The *dy* mutation has been propagated by self-fertilization for many decades and is presumed to be in an isogenic, *albeit* undefined, genetic background. We did notice, however, that the *dy* gene produced two different transcripts, the canonical one, *ZmSUN3* (Murphy et al,. 2010), and a less abundant splice variant here designated *ZmSUN3-sv1* (Fig. 7C, transcripts labeled 'sv1'). The splice variant results from intron 3 retention, and the resulting mRNA would encode a shorter protein that lacks the two C-terminal transmembrane domains. Accumulation of this truncated SUN3 protein in the meiotic nucleus could disrupt the targets, folding, or interactions of SUN3 with its normal partners. Such a scenario would be compatible with the *dy* phenotypes observed, especially the precocious telomere detachment and the NE distortion. In this scenario (Fig. 7F), accumulation of aberrant SUN3 protein could disrupt its meiotic function. To investigate this possibility further, we amplified SUN3 cDNA from normal and *dy* male flowers at meiosis stage and found that the splice variant was the most abundant form in *dy* (Fig. 7E). We also observed the

SUN3-sv1 transcript in non-meiotic tissues and other genotypes, but to a lesser relative degree (not shown), consistent with random EST reads performed by others (Fig. 7C).

The presence of the variant transcript and it's increased proportion in *dy/dy* anthers, we consider a possible scenario in which *dy* is a gain-of-function, antimorphic mutation resulting from a splice variant that accumulates to detrimental levels in the homozygous (*dy/dy*) or hemizygous (*dy*/-) plants, but not in heterozygous (+/-) or wild-type (+/+) plants. We suggest, therefore, that the splice variant of SUN3 may be the basis for the mutant phenotypes observed.

Finally, we recognize that other genes besides SUN3 that reside in the linkage deserve careful consideration. These other candidate genes are listed in Figure 8 alongside a diagrammatic summary of a hypothetical meiotic SUN LINC complex. We considered genetic disruption of processes that involve gene products in any of three cellular domains: the cytoplasm, the nuclear envelope, and the nucleoplasm. In the cytoplasm, candidate genes would include components of the motility system, such as tubulin or actin; molecular motors; or connector proteins that link these to the nuclear envelope. In the nuclear envelope, candidate genes would include KASH and SUN domain proteins. In the nucleoplasm, candidate genes are more numerous, reflecting the abundance of structural and enzymatic gene products required for meiosis. Finally, we considered candidate genes for regulatory control or any of these processes in a meiotic SUN LINC complex pathway, such as check point or signal transduction genes. Overall, considering all of these candidates, we find that SUN3 is the most compelling candidate and favor the hypothesis that the mutant phenotypes of *dy* are caused by an allele of SUN3 that imparts a disruptive gain-of-function to the meiotic nuclear envelope.

Discussion

In the current study, we have undertaken a detailed 3D cytological analysis of *dy* and discovered several new phenotypes that place it in a pathway integrating NE functions with meiotic chromosome segregation. Collective, our newly discovered *dy* phenotypes—(1) incomplete telomere clustering in early prophase, (2) defects in progression of synapsis as revealed by ASY1 immunostaining, (3) marked nuclear morphology distortion using nuclear shape analysis, and (4) anaphase bridges—show that *dy* is pleiotropic and may involve direct or indirect disruption of a LINC complex-like pathway that operates during meiotic prophase in maize.

Our immunofluorescence staining of ASY1 provided clear evidence of synaptic irregularities. The ASY1 antibody was raised against a recombinant protein made from an ASY1 cDNA of Arabidopsis (Armstrong et al., 2002) and shown to detect chromosome axis in meiosis of other plant species including maize (Golubovskaya et al., 2006). This antiserum has previously been used successfully to characterize defects in synapsis in other maize mutants (Golubovskaya et al., 2011). The ASY1 protein associates with the chromosomal axis of unsynapsed meiotic chromosome fibers and is thought to be removed from the chromosomes as they synapse (Armstrong et al., 2002; Sanchez-Moran et al., 2008; Sanchez-Moran et al., 2007). This pattern is seen for wild-type maize in this study (Fig. 2B and 2E) but not for *dy*, where persistent ASY1 staining is believed to indicate incomplete synapsis leading to asynapsis. This view differs slightly from previously published descriptions of the mutant, in which the

homologs synapse and exhibit a normal pachytene but fail to maintain chiasmata (Maguire et al., 1991), unless complete synapsis in *dy* is followed by partial desynapsis and ASY1 reloading.

Another possible explanation for the ASY1 staining pattern in *dy* is that the processing or resolution of meiotic chromosome tangles or interlocks is affected by the mutation. Disruption of interlock resolution could leave physical barriers to the formation of complete synaptonemal complexes, such as those described by Maguire et al. (1991). Exactly how the completion of synapsis is monitored by the cell in maize meiosis remains unknown, but incomplete synapsis could trigger checkpoints or affect feedback loops. In addition, we note that any of these defects—asynapsis, desynapsis, or interlock resolution—could occur simultaneously and to different degrees in individual *dy* nuclei. Regardless of the mechanism, our findings of the effect of *dy* on nuclear shape distortion establish a functional link between meiotic chromosome metabolism inside the nucleus and organelle integrity and likely cytoplasmic forces operating on or outside of the nucleus. Other mutants of maize, such as *pam1* (Golubovskaya et al., 2002; Golubovskaya and Mashnenkov, 1977), also link telomere positioning to meiotic chromosome segregation, suggesting that the *Pam1* gene also functions in the NE-telomere-synapsis pathway described here for *dy*. Indirect evidence that is consistent with our distortion-detachment model (Fig. 7F) comes from a recent study on Arabidopsis SUN proteins, shown to play a role in somatic nuclear morphology in part through a SUN-KASH, LINC complex-type mechanism (Zhou et al., 2012).

Maize has historically been an excellent model system for forward genetic studies. Over 50 meiotic mutants of maize have been isolated (representing at least 35

different genetic loci), but only 14 have been genetically mapped, and still fewer (*n* = *6*) have actually been cloned and characterized (Cande et al., 2009; Golubovskaya et al., 2003). We have mapped another historical maize meiotic mutant, *desynaptic (dy),* to a region on chromosome 3L, bin 3.06, using two B-A translocation mapping stocks and an SSR-based BSA mapping strategy. The requirement for cytological verification in progeny F3 families (Fig. 5) limited the mapping resolution in our study to a 7.7-Mbp region (Fig. 6, 7).

Maize *dy* has previously been defined as a recombination modifier gene (Ji et al., 1999). Relatedly, genetic control of recombination frequency in maize was subjected to QTL mapping by two groups, and in each study, the biggest effect QTL mapped to regions immediately adjacent to our *dy* mapping interval (Dole and Weber, 2007; Esch et al., 2007). These map positions were estimated to be between 166.0 and 168.5 MB (Esch et al., 2007) and at 181.1 MB (Dole and Weber, 2007) on the physical map of maize, which map just beyond our proximal and distal boundaries, respectively. Interestingly, the QTL with the greatest effect on recombination in Arabidopsis mapped near the end of chromosome 1, a region including At1G71360, predicted to encode a PM3-type SUN-domain.

A key to positional map-based cloning is the availability of other alleles for validation of candidate genes. To date, only one other mutation has been shown to be similar to *dy*, namely *desynaptic1* (*dsy1*, Golubovskaya et al., 1997). Maguire and Jackson (1998) carried out allelism test crosses between *dsy1* and *dy*. They described the progeny as having normal-looking pachytene, metaphase I, anaphase I, and quartet stage cells, yet concluded that they were allelic on the basis of a variant diakinesis

phenotype. Some alleles might possibly partially complement each other, or the progeny might be nonallelic but, in double heterozygous form, reveal a subtle diakinesis phenotype. Indeed, we favor requiring a stricter definition of allelism, in which primary phenotypes, such as univalents and micronuclei, would be present and conspicuous in the male meiocytes of test-cross progeny. In this regard, we would expect *dsy1* mapping to reveal a locus unlinked to *dy* on 3L.

From our initial screen for candidate genes, we identified a novel protein-coding gene predicted to encode a SUN domain-containing protein. Although we failed to detect a genetic lesion in this gene at the genomic DNA level, we have evidence for the existence of a significant amount of a splice variant predicted to encode a truncated protein lacking its two C-terminal transmembrane domains. Further experiments with qRT-PCR will allow for a more quantifiable detection of this transcript from different lines of maize. We hypothesize that, given enough available unspliced mRNA product, the translated protein is likely to be unable to carry out one or more essential cellular functions, including either telomere tethering to the NE or NE-cytoplasmic force transduction. The overall phenotypes observed with *dy* bear a striking similarity to those of *MmSun1* knockout mice, in which meiotic telomere-NE detachment precedes meiotic failure and sterility (Ding et al., 2007).

If the aberrant transcript, *Sun3-sv1*, is causing the mutant phenotype, it might explain the variable expressivity observed with homozygous *dy*. In this case, *ZmSUN3-sv1* RNA levels may have to accumulate to a critical threshold level to disrupt recombination and subsequent disjunction of homologs. This accumulation could produce a gain-of-function antimorphic mutation, for which similar alleles would be

relatively rare. Alternatively, we have considered the possibility that *SUN3* is a dying pseudogene, producing aberrant transcripts or even anti-sense transcripts that could contribute to gene silencing of *ZmSUN3* or its closely related unlinked duplicate gene, *ZmSUN4*. Finally, it is possible that the *dy* mutation may be located not in the *SUN3* gene but in another nearby gene, such as one of the candidates listed in Fig. 8. Among these other candidates are genes whose products could function in a LINC complex–type pathway. These include genes encoding Actin-2, Beta tubulin, pleckstrin-homology domain, and MAR-binding filament-like proteins. These genes represent targets for reverse genetic analysis, in which meiosis-specific knockout or knockdowns would be expected to disrupt nuclear morphology, telomere positioning, synaptic progression, and eventual meiotic chromosome segregation. Further genetic and molecular analysis of *Dy* and its interacting partners is expected, therefore, to open new avenues for exploration of the intricate processes at work in meiotic cells.

513 **Acknowledgements**

514 We thank the members of the Bass laboratory, including A. Brown, E. S. Howe, and D.

515 Vera, for critical reading of the manuscript and insightful comments. We thank A. B.

516 Thistle for editing the manuscript. This work was supported by an AHA Pre-doctoral

517 fellowship to SPM (# 0715487B), funding from the NSF (MCB-0091095; IOS-1025954),

518 and a Florida State University CRC-Planning Grant to HWB.

References

Abramoff, M. D., Magalhaes, P. J. and Ram, S. J. (2004). Image processing with ImageJ. *Biophotonics Int.* 11, 36–42.

Armstrong, S. J., Caryl, A. P., Jones, G. H., and Franklin, F. C. (2002). Asy1, a protein required for meiotic chromosome synapsis, localizes to axis-associated chromatin in *Arabidopsis* and *Brassica. J. Cell Sci*. 115, 3645–3655.

Bass, H. W. (2003). Telomere dynamics unique to meiotic prophase: formation and significance of the bouquet. *Cell. Mol. Life Sci*. 60, 2319–2324.

Bass, H. W., Marshall, W. F., Sedat J. W., Agard, D. A. and Cande, W. Z. (1997). Telomeres cluster de novo before the initiation of synapsis: a three-dimensional spatial analysis of telomere positions before and during meiotic prophase. *J. Cell Biol*. 137, 5–18.

Bass, H. W., Bordoli, S. J. and Foss, E. M. (2003). The *desynaptic (dy)* and *desynaptic1 (dsy1)* mutations in maize (*Zea mays* L.) cause distinct telomere-misplacement phenotypes during meiotic prophase. *J. Exp. Bot*. 54, 39–46.

Beckett, J. B. (1978). B-A translocations in maize. 1. Use in locating genes by chromosome arms. *J. Hered*. 69, 27–36.

Bennett, M. D. 1977. The time and duration of meiosis. *Philos. Trans. R. Soc. Lond. B Biol. Sci*. 277, 201–226.

Cande, W. Z., Golubovskaya, I., Wang, R. and Harper, L. (2009). Meiotic genes and meiosis in maize. In *The Maize Handbook II: Genetics and Genomics* (ed. J. L. Bennetzen and S. Hake), pp. 353-373. New York: Springer.

Caryl, A. P., Armstrong, S. J., Jones, G. H. and Franklin, F. C. (2000). A homologue of the yeast HOP1 gene is inactivated in the *Arabidopsis* meiotic mutant *asy1. Chromosoma* 109, 62–71.

Chang, M. T. and Neuffer, M. G. (1989). Maize microsporogenesis. *Genome* 32, 233–243.

Chikashige, Y. and Hiraoka, Y. (2001). Telomere binding of the Rap1 protein is required for meiosis in fission yeast. *Curr. Biol.* 11, 1618–1623.

Conrad, M. N., Lee, C. Y., Wilkerson, J. L. and Dresser, M. E. 2007. MPS3 mediates meiotic bouquet formation in *Saccharomyces cerevisiae. Proc. Natl. Acad. Sci. USA* 104, 8863–8868.

Cooper, J. P., Watanabe, Y. and Nurse, P. (1998). Fission yeast Taz1 protein is required for meiotic telomere clustering and recombination. *Nature* 392, 828–831.

Davis, G. L., McMullen, M. D., Baysdorfer, C., Musket, T., Grant, D., Staebell, M., Xu, G., Polacco, M., Koster, L., Melia-Hancock, S. et al. (1999). A maize map standard with sequenced core markers, grass genome reference points and 932 expressed sequence tagged sites (ESTs) in a 1736-locus map. *Genetics* 152, 1137–1172.

Dellaporta, S. L., Wood, J. and Hicks, J. B. (1985). Maize DNA miniprep. *Plant Mol. Biol. Rep.* 30, 36–38.

Ding, X., Xu, R., Yu, J., Xu, T., Zhuang, Y. and Han, M. (2007). SUN1 is required for telomere attachment to nuclear envelope and gametogenesis in mice. *Dev. Cell* 12, 863–872.

Dole, J. and Weber, D. F. (2007). Detection of quantitative trait loci influencing recombination using recombinant inbred lines. *Genetics* 177, 2309–2319.

Esch, E., Szymaniak, J. M., Yates, H., Pawlowski, W. P. and Buckler, E. S. (2007). Using crossover breakpoints in recombinant inbred lines to identify quantitative trait loci controlling the global recombination frequency. *Genetics* 177, 1851–1858.

Franklin, A. E., Golubovskaya, I. N., Bass, H. W. and Cande, W. Z. (2003). Improper chromosome synapsis is associated with elongated RAD51 structures in the maize *desynaptic2* mutant. *Chromosoma* 112, 17–25.

Golubovskaya, I. N. and Mashnenkov, A. S. (1977). Multiple disturbances of meiosis in corn caused by a single recessive mutation pamA-A344. *Genetika* 13, 1910–1931.

Golubovskaya, I. N., Harper, L. C., Pawlowski, W. P., Schichnes, D. and Cande, W. Z. (2002). The *pam1* gene is required for meiotic bouquet formation and efficient homologous synapsis in maize (*Zea mays* L.). *Genetics* 162, 1979–1993.

Golubovskaya, I., Sheridan, W., Harper, L. and Cande, W. Z. (2003). New meiotic mutants of maize identified from Mu transposon and EMS mutant screens. *Maize Genet. Coop. Newsl.* 77, 10–13.

Golubovskaya, I. N., Hamant, O., Timofejeva, L., Wang, C. J., Braun, D., Meeley, R. and Cande, W. Z. (2006). Alleles of *afd1* dissect REC8 functions during meiotic prophase I. *J. Cell Sci.* 119, 3306–3315.

Golubovskaya, I. N., Wang, C. J., Timofejeva, L. and Cande, W. Z. (2011). Maize meiotic mutants with improper or non-homologous synapsis due to problems in pairing or synaptonemal complex formation. *J. Exp. Bot*. 62, 1533–1544.

Graumann, K., Runions, J. and Evans, D. E. (2010). Characterization of SUN-domain proteins at the higher plant nuclear envelope. *Plant J*. 61, 134–144.

Harper, L., Golubovskaya, I. and Cande, W. Z. (2004). A bouquet of chromosomes. *J. Cell Sci*. 117, 4025–4032.

Hiraoka, Y. and Dernburg, A. F. (2009). The SUN rises on meiotic chromosome dynamics. *Dev. Cell* 17, 598–605.

Ji, Y., Stelly, D. M., De Donato, M., Goodman, M. M. and Williams, C. G. (1999). A candidate recombination modifier gene for *Zea mays* L. *Genetics* 151, 821–830.

John, B. (Ed.) (1990). Meiosis. *Developmental and Cell Biology Series* **22**. Cambridge University Press, New York. 396 pp.

Lawrence, C. J., Seigfried, T. E., Bass, H. W., and Anderson, L.K. (2006). Predicting chromosomal locations of genetically mapped loci in maize using the Morgan2McClintock translator. *Genetics* 172, 2007–2009.

Maguire, M. P., and Jackson, J. D. (1998). Two well-known mutants of chiasma maintenance function in maize are allelic. *Genome* 41, 417-421.

Maguire, M. P., Paredes, A. M. and Riess, R. W. (1991). The desynaptic mutant of maize as a combined defect of synaptonemal complex and chiasma maintenance. *Genome* 34, 879–887.

Maguire, M. P., Riess, R. W. and Paredes, A. M. (1993). Evidence from a maize desynaptic mutant points to a probable role of synaptonemal complex central

region components in provision for subsequent chiasma maintenance. *Genome* 36, 797–807.

Michelmore, R. W., Paran, I., and Kesseli, R. V. (1991). Identification of markers linked to disease-resistance genes by bulked segregant analysis: a rapid method to detect markers in specific genomic regions by using segregating populations. *Proc. Natl. Acad. Sci. USA* 88, 9828–9832.

Mikhailova, E. I., Phillips, D., Sosnikhina, S. P., Lovtsyus, A. V., Jones, R. N. and Jenkins, G. (2006). Molecular assembly of meiotic proteins Asy1 and Zyp1 and pairing promiscuity in rye (*Secale cereale* L.) and its synaptic mutant *sy10. Genetics* 174, 1247–1258.

Moriguchi, K., Suzuki, T., Ito, Y., Yamazaki, Y., Niwa, Y. and Kurata, N. (2005). Functional isolation of novel nuclear proteins showing a variety of subnuclear localizations. *Plant Cell* 17, 389–403.

Murphy, S. P. and Bass, H. W. (2012). Genetics and cytology of meiotic chromosome behavior in plants. In *Plant Genetics and Genomics: Crops and Models. Vol. 4* (ed. H. W. Bass and J. W. Brichler), pp. 193–229. New York: Springer.

Murphy, S. P., Simmons, C. R. and Bass, H. W. (2010). Structure and expression of the maize (*Zea mays* L.) SUN-domain protein gene family: evidence for the existence of two divergent classes of SUN proteins in plants. *BMC Plant Biol*. 10, 269.

Nelson, O. N. and Clary, G. B. 1952. Genic control of semi-sterility in maize. *J. Hered.* 43, 205–210.

Oda, Y. and Fukuda, H. (2011). Dynamics of *Arabidopsis* SUN proteins during mitosis and their involvement in nuclear shaping. *Plant J*. 66, 629–641.

Pawlowski, W. P., Wang, C. J., Golubovskaya, I. N., Szymaniak, J. M., Shi, L., Hamant, O., Zhu, T., Harper, L., Sheridan, W. F. and Cande, W. Z. (2009). Maize AMEIOTIC1 is essential for multiple early meiotic processes and likely required for the initiation of meiosis. *Proc. Natl. Acad. Sci. USA* 106, 3603–3608.

Sanchez-Moran, E., Santos, J. L., Jones, G. H. and Franklin, F. C. (2007). ASY1 mediates AtDMC1-dependent interhomolog recombination during meiosis in *Arabidopsis. Genes Dev*. 21, 2220–2233.

Sanchez-Moran, E., Osman, K., Higgins, J. D., Pradillo, M., Cunado, N., Jones, G. H. and Franklin, F. C. (2008). ASY1 coordinates early events in the plant meiotic recombination pathway. *Cytogenet. Genome Res*. 120, 302–312.

Scherthan, H. (2007). Telomere attachment and clustering during meiosis. *Cell Mol. Life Sci*. 64, 117–124.

Scherthan, H. (2009). Analysis of telomere dynamics in mouse spermatogenesis. *Methods Mol. Biol*. 558, 383–399.

Scherthan, H., Weich, S., Schwegler, H., Heyting, C., Harle, M. and Cremer, T. (1996). Centromere and telomere movements during early meiotic prophase of mouse and man are associated with the onset of chromosome pairing. *J. Cell Biol*. 134, 1109–1125.

Schmitt, J., Benavente, R., Hodzic, D., Hoog, C., Stewart, C. L. and Alsheimer, M. (2007). Transmembrane protein Sun2 is involved in tethering mammalian

meiotic telomeres to the nuclear envelope. *Proc. Natl. Acad. Sci. USA* 104, 7426–7431.

Starr, D. A. (2009). A nuclear-envelope bridge positions nuclei and moves chromosomes. *J. Cell Sci*. 122, 577–586.

Starr, D. A. and Fridolfsson, H. N. (2010). Interactions between nuclei and the cytoskeleton are mediated by SUN-KASH nuclear-envelope bridges. *Annu. Rev. Cell Dev. Biol*. 26, 421–444.

Trelles-Sticken, E., Dresser, M. E. and Scherthan, H. (2000). Meiotic telomere protein Ndj1p is required for meiosis-specific telomere distribution, bouquet formation and efficient homologue pairing. *J. Cell Biol*. 151, 95–106.

Van Damme, D., Bouget, F. Y., Van Poucke, K., Inze, D. and Geelen, D. (2004). Molecular dissection of plant cytokinesis and phragmoplast structure: a survey of GFP-tagged proteins. *Plant J*. 40, 386–398.

Wang, C. J., Carlton, P. M., Golubovskaya, I. N. and Cande, W. Z. (2009). Interlock formation and coiling of meiotic chromosome axes during synapsis. *Genetics* 183, 905–915.

Zhou, X., Graumann, K., Evans, D. E. and Meier, I. (2012). Novel plant SUN-KASH bridges are involved in RanGAP anchoring and nuclear shape determination. *J. Cell Biol.* 196, 203–211.

Figure Legends

Fig. 1. 3D telomere FISH in normal and *dy* nuclei at the zygotene stage of meiosis. Male meiotic cells from normal (+/+, inbred line A344, panels A–D) and mutant (*dy/dy*, panels E–H) bouquet-stage formaldehyde-fixed meiotic cells were subjected to 3D acrylamide telomere FISH. 3D data from individual nuclei were collected, deconvolved, and displayed as maximum-intensity through-focus projections revealing the chromatin (DAPI; panels A, E), telomere FISH signals (FITC; panels B, F), or both as pseudocolor overlay images (MERGE; red DAPI, green FITC; panels C, G). Telomere FISH signals for these two nuclei are displayed separately as 3D model projections (panels D, H) with the nucleus outline traced as red polygons and the FISH signals displayed as green (representing telomeres at the nuclear periphery) or yellow (telomeres in the nuclear interior). The normal nucleus shows the typical wild-type telomere cluster/bouquet phenotype, in which the majority of telomeres clustered on one area of the nuclear periphery. The mutant (*dy/dy*) nucleus shows partial bouquet phenotype, with a *dy*-specific telomere mislocalization phenotype (F, arrows; H, yellow signals).

Fig. 2. ASY1 immunostaining in normal and *dy* nuclei at the zygotene and pachytene stages of meiosis. (A–F) Male meiotic cells from normal (+/+, inbred line A344) mid-prophase formaldehyde-fixed anthers subjected to 3D acrylamide immunolocalization with ASY1 antisera. (G–L) Mutant (*dy/dy*) cells treated in the same way. 3D data were collected, deconvolved, and displayed as described for Fig. 1. Normal (+/+) nuclei at zygotene (A–C) and pachytene (D–F) show typical wild-type

694 phenotypic staining patterns for ASY1, detected along chromosome fiber axes at
695 zygotene (B), but not at pachytene (C), when synapsis is complete. Mutant nuclei
696 (*dy*/*dy*) show normal ASY1 staining at zygotene (G–I, compare panel H to B) but a *dy*-
697 specific detection of ASY1 staining of long and short segments at pachytene (J–L,
698 arrows in K and compare panel K to E).
699
700 **Fig. 3. Nuclear shape analysis in normal and *dy* meiotic nuclei.** Nuclear shape
701 analysis in normal (A344, A–C, and KYS, D–F) and *dy* (G–U) nuclei (from the F4
702 generation of a mapping population derived from KYS x *dy*) at the pachytene stage of
703 meiosis. Degree of circularity for nuclei from 3D datasets collected for immunostaining
704 or immuno-FISH experiments derived from periphery tracings made on a 3-section (0.9
705 µm) projection from the middle region of the data. DAPI images show whole-nucleus
706 projections (A–I) together with the nuclear shape image resulting from edge tracing on
707 the central 0.9-µm projection. Nuclear shape images alone (J–U) are shown for an
708 additional 12 *dy* nuclei illustrating the *dy*-specific phenotype of nuclear morphology
709 alteration. The periphery trace polygons were imported into image J, and the degree of
710 circularity (V) and aspect ratio's (W) were determined and summarized in the
711 histograms for the indicated genotypes. Tukey's post-hoc multiple comparison test
712 results indicate significant differences for *dy* (**). Error bars represent standard error of
713 the mean.
714
715 **Fig. 4 Chromosome bridges, laggards, and micronuclei after meiotic prophase.**
716 DAPI images (A–J) of male meiotic cells from normal (+/+, A–E) or mutant (*dy/dy*, F–J)

formaldehyde-fixed anthers after acrylamide embedding and DAPI staining. Stages of meiosis are indicated across the top, and each image is a through-focus projection of the entire dataset. Normal cells exhibit typical patterns of chromosome arrangement at anaphase I (A) telophase I (B, C), prophase II (D), and postmeiotic stage showing the four daughter cells (tetrad, E) of a single meiotic prophase. Mutant *dy*-specific chromosome missegregation phenotypes are evident at all of these same stages. Mutant phenotypes shown include anaphase bridges (F, arrow), lagging chromosomes (G, arrows), and micronuclei (H–J, arrows), all of which contribute to the characteristic increase in aneuploidy and sterility associated with the *dy* mutants.

Fig. 5. Diagram of *dy* linkage mapping population production and use for bulked-segregant analysis. An F2 mapping population was produced by means of conventional monohybrid cross with the wild-type (WT) parent as the mother (P1, +/+, genotype KYS) and the mutant parent as the father. We also selfed individual F2 plants to produce F3 generation families to determine which F2 individuals were *dy/dy* homozygous mutants before bulked-segregant linkage mapping.

Fig. 6 Linkage mapping of *dy* to the long arm of chromosome 3, in genetic bin 3.06. Maps from B-A translocations (A) and BSA (B–D) mapping experiments are shown. Two different B-A translocation stocks uncovered the *dy* mutant phenotype (by means of the chromosome missegregation phenotypic assay illustrated in Fig. 4). Haploid regions used to uncover loci on chromosome 3 are indicated (A, dashed lines) for two different B-A translocation stocks (Tb-3La, Tb-3La-2s (6270)). BSA mapping

placed *dy* in genetic bin 3.06 (B, *dy* interval bracketed on the UMC 1998 3 genetic linkage map from Davis et al., 1999). The BSA and follow-up SSR mapping interval was narrowed to a region between markers *umc1730/zmm16* and *bnlg1047a*, as indicated or extrapolated for two additional common linkage maps (C, "Genetic 2008 3", and D, "IBM2 2008 Neighbors 3"). The *dy* mapping interval, along with the location of a candidate gene, *ZmSUN3,* is indicated on the last two maps (C, D), which show the locations and centiMorgan values of shared markers and extrapolated estimates (parentheses). Grey boxes (B) indicate two QTL involved in meiotic recombination control.

Fig. 7. Candidate gene analysis of the maize *SUN3* protein gene. The *dy* mapping interval (A) (~8.12 MB) identified and (B) associated genes and gene models. The red box indicates our highest-ranked candidate gene, *ZmSUN3* (screen capture from maizesequence.org., B73 RefGen_v2 sequence). The full-length *ZmSUN3* is physically split between two BACs (C), AC195254 and AC211274 (blue lines). 14 ESTs (C) mapped to this genomic region are indicated; *sv1 indicates intron 3–retained cDNAs (screen capture from www.plantgdb.org., B73 RefGen_v2 sequence). The predicted genomic DNA structures for *ZmSUN3* and *ZmSUN3-sv1* (D), from Murphy et al. (2010), including exons (Ex) and introns (I) are shown. Genomic (blue) and cDNA clones (pink) are listed under the gene structures with the genotypes indicated in parentheses. RT-PCR and agarose gel analysis (E) of *ZmSUN3* from total RNA isolated from *dy/dy* and KYS+/+ meiotic anthers resulted in two bands; the intron 3–retained (arrow) and the intron 3–spliced (arrow heads) mRNA's are detectable in both genotypes but to a much

greater extent in *dy* maize lines. The predicted proteins and associated predicted domains from each of these splice variants are shown (T = transmembrane domain, SUN = Sad1/Unc-84 domain, P = Pad domain from Murphy et al. (2010), C= coiled-coil domain). (F) A model for the disruption of the telomeres from the nuclear periphery and how it could lead to nuclear deformation and chromosome missegregation**.**

Fig. 8. Hypothetical meiotic SUN LINC complex and candidate genes near *dy*. (A) Cytoskeletal motility systems including microtubules, actin, and intermediate filaments are associated via unknown connectors (black boxes) with the nuclear envelope (NE) via (B) ONM-associated KASH and (inner nuclear membrane) INM-associated SUN proteins. (C) The nucleoplasm and SUN-mediated telomere attachment and movement are indicated. Other genes linked to *dy* (right panel) that encode proteins involved in either the cytoplasm, NE, DNA/chromatin metabolism, and regulatory complexes along with associated GRMZM gene identification are indicated.

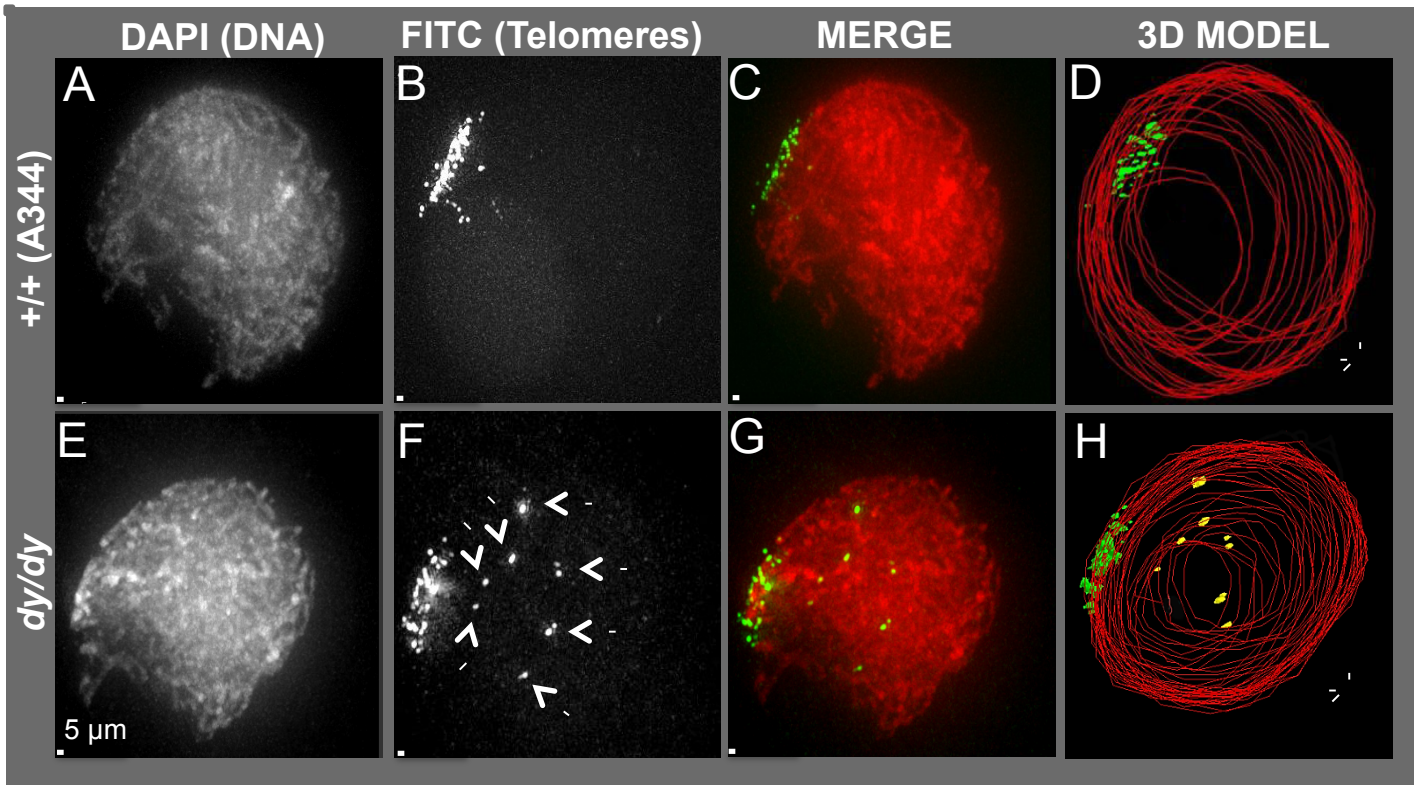

Figure 1, Murphy and Bass

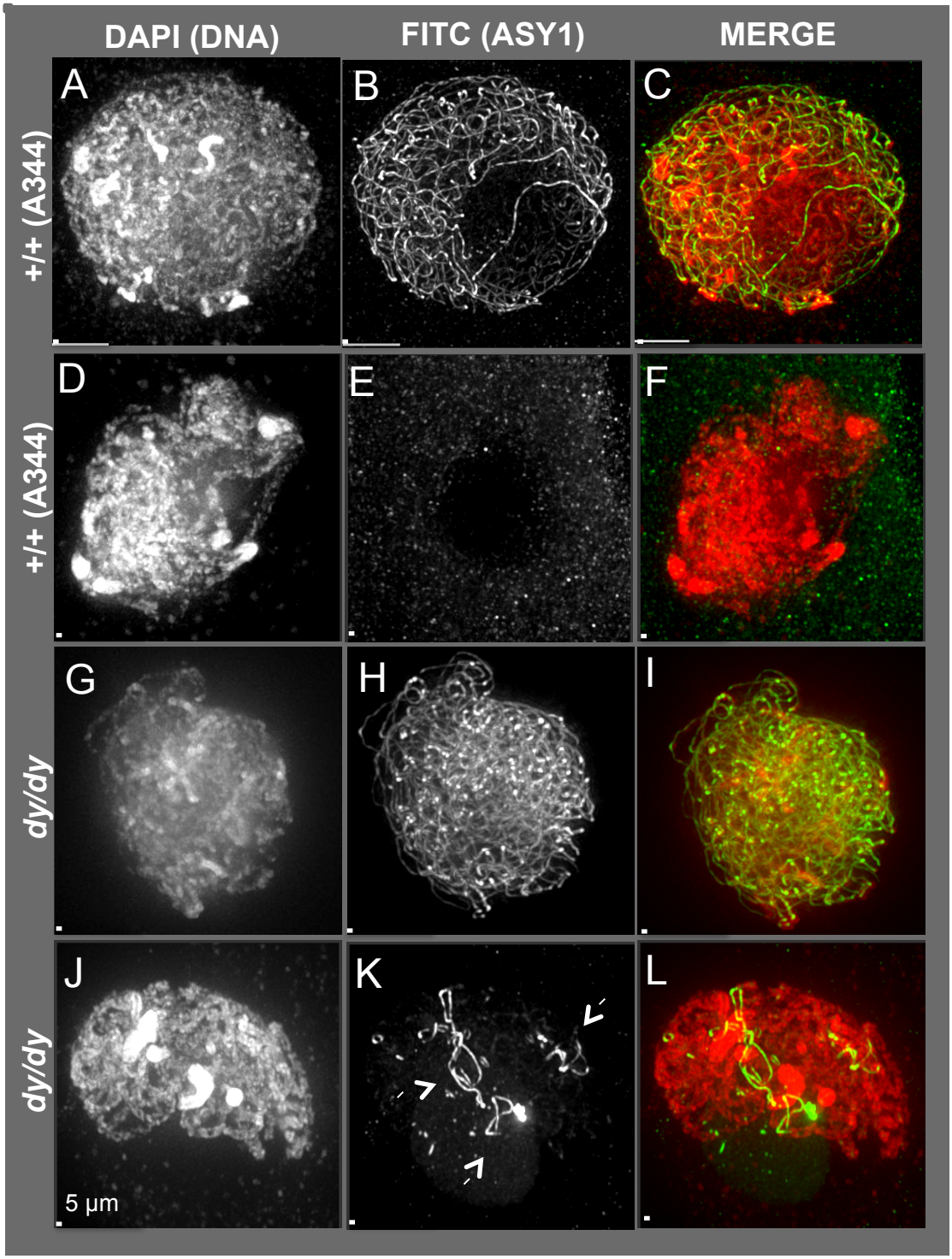

Figure 2, Murphy and Bass

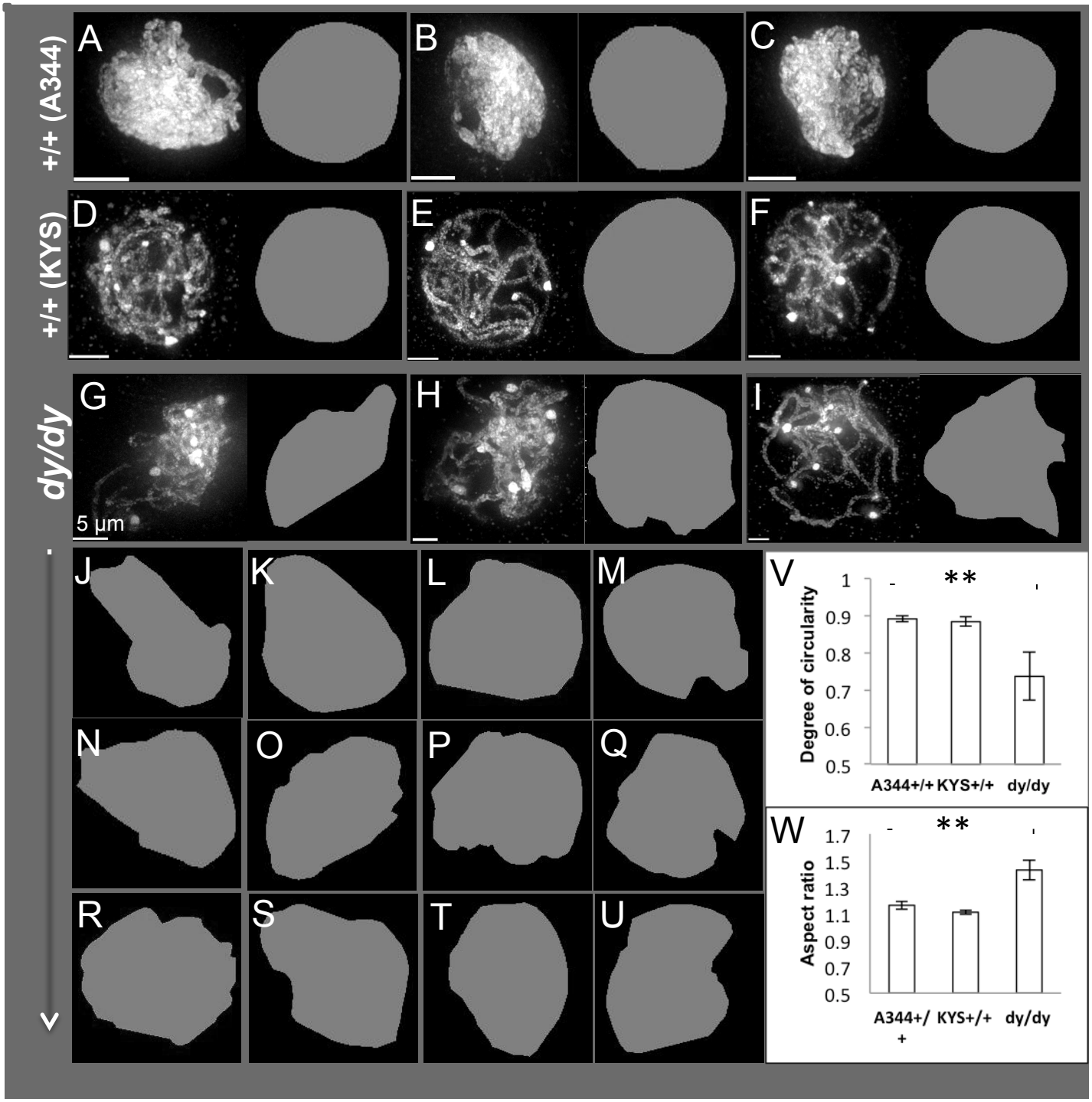

Figure 3, Murphy and Bass

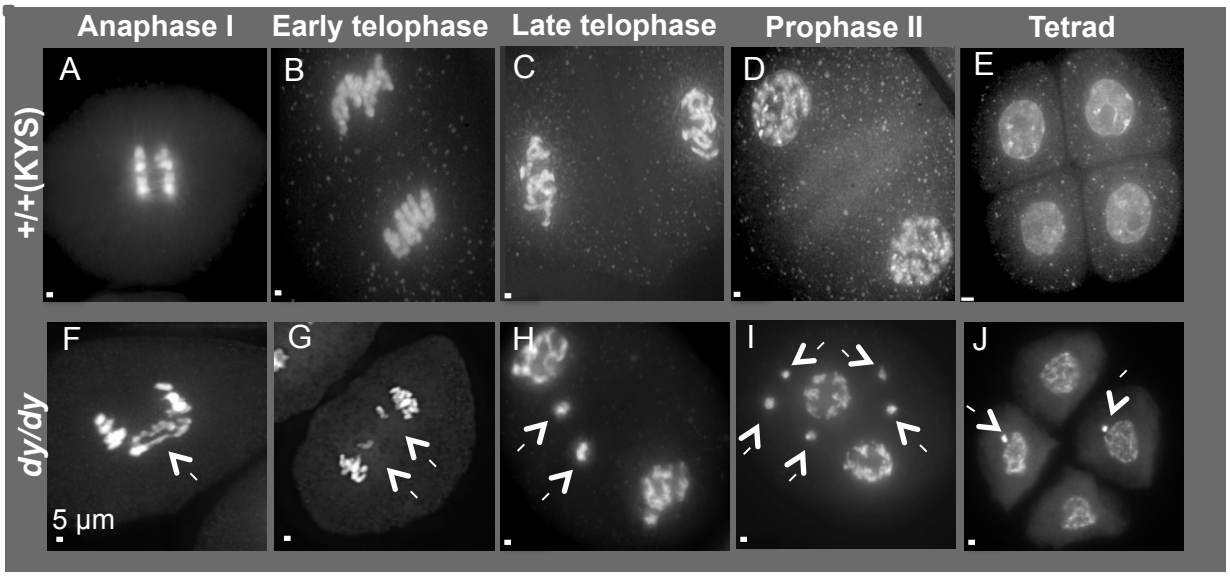

Figure 4, Murphy and Bass

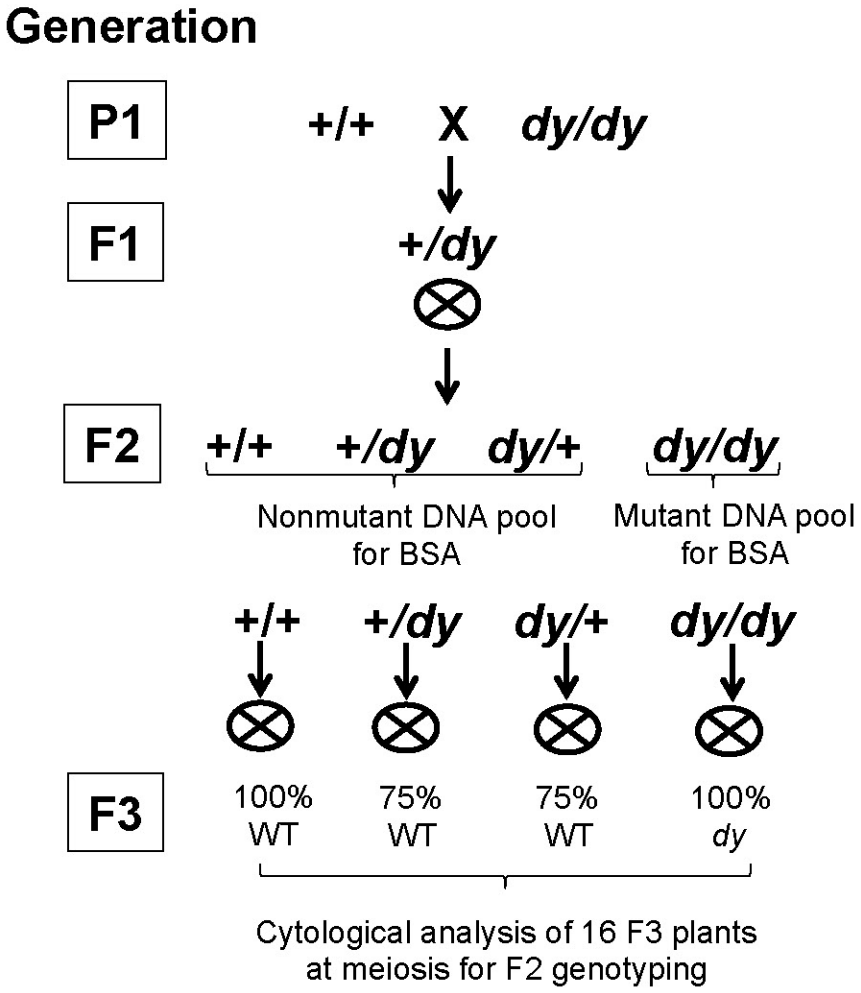

Figure 5, Murphy and Bass

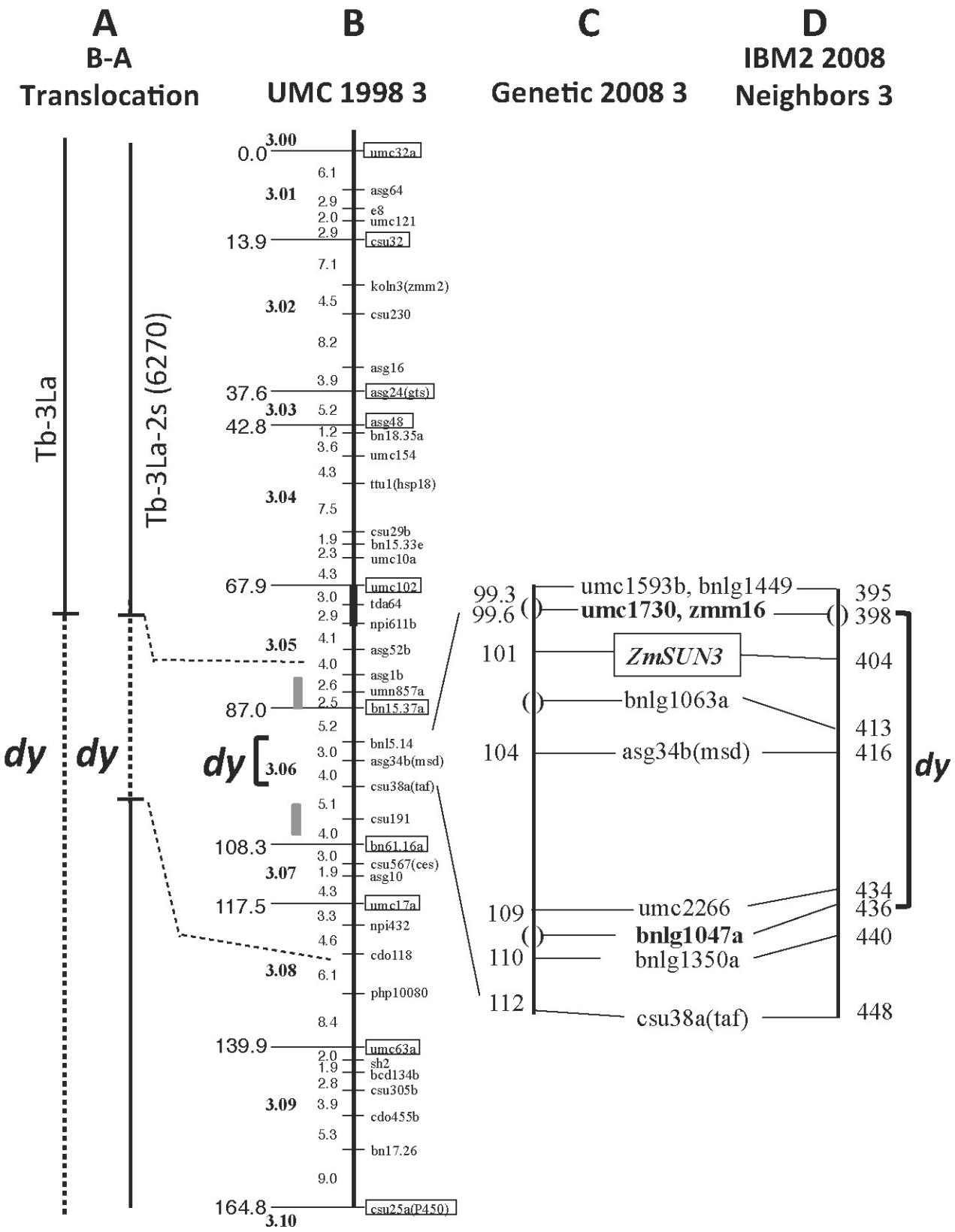

Figure 6, Murphy and Bass

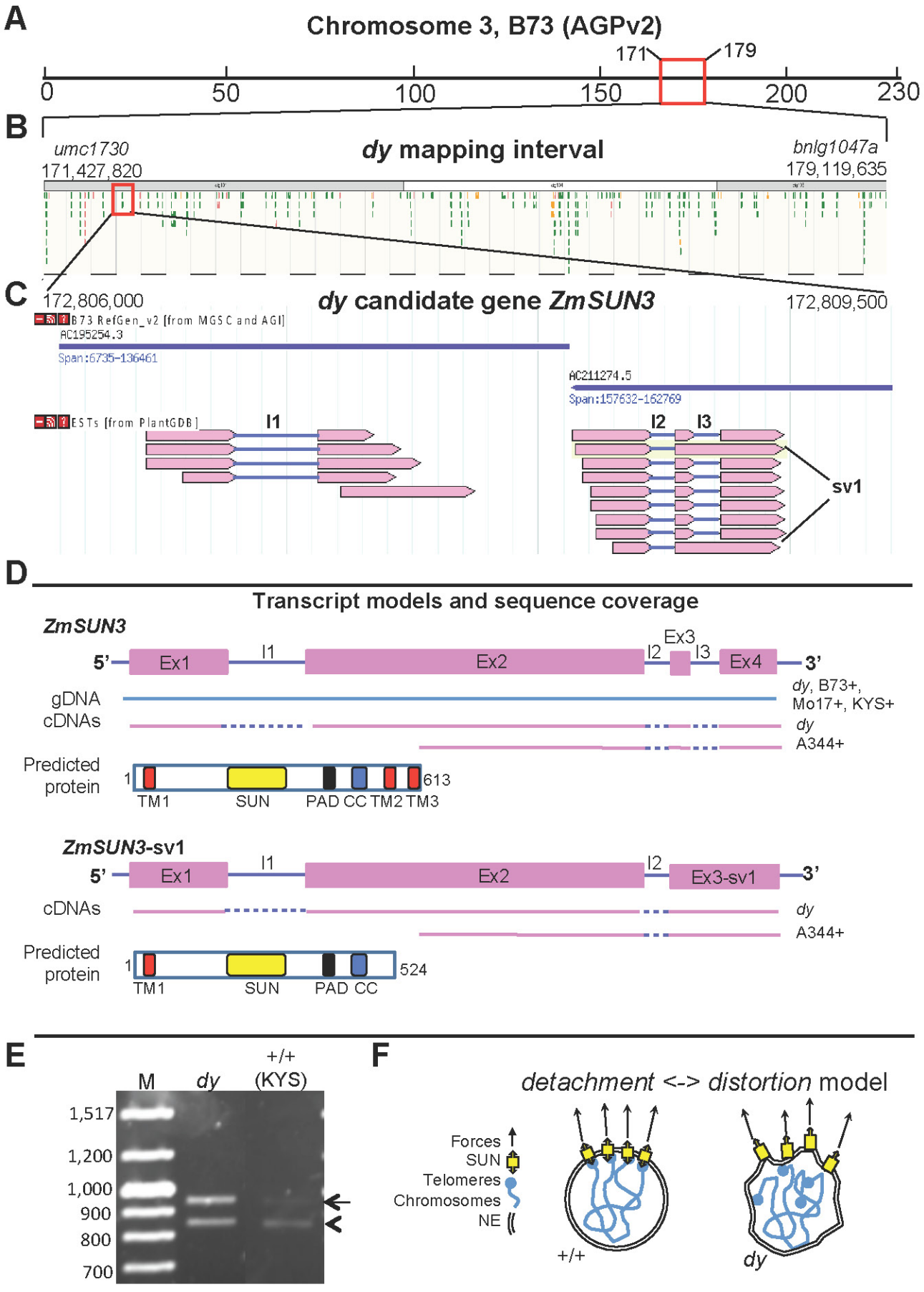

Figure 7, Murphy and Bass

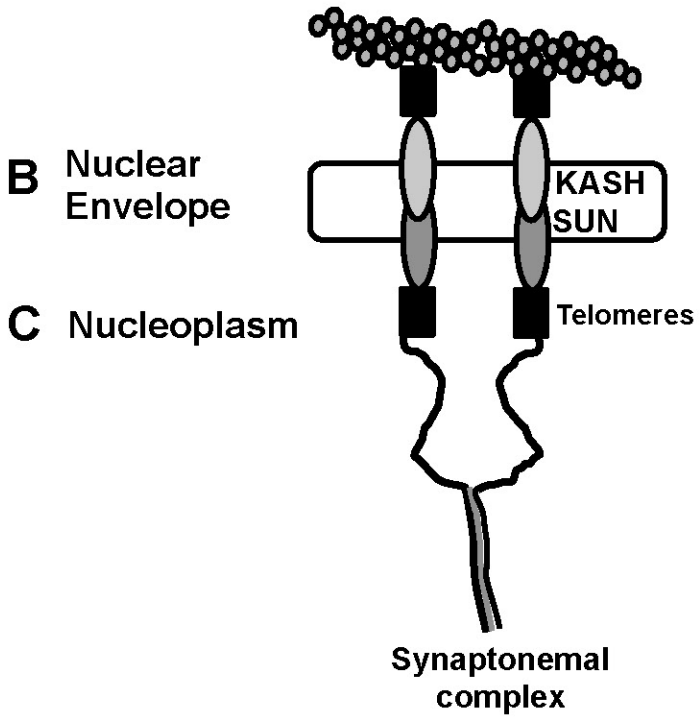

	Predicted Protein
Cytoskeleton	
AC210312.3_FG005	Beta tubulin
GRMZM2G053284	Actin-2/ ACT2
GRMZM2G128918	PH domain-containing protein
Nuclear Envelope	
Fig. 7D	ZmSUN3, ZmSUN3-sv1
Nucleoplasm	
GRMZM2G110072	MAR-binding filament-like protein
GRMZM2G049373	Pollen-specific DnaJ-like protein
GRMZM2G081519	DNA polymerase I
GRMZM2G129428	Nucleic acid binding protein
GRMZM2G305793	DNA repair protein XRCC2 homolog
GRMZM2G320360	DNA topoisomerase I
GRMZM2G149802	DNA polymerase
GRMZM2G078314	Histone H3
GRMZM2G027914	Myb/SANT
GRMZM2G096802	ERCC-8 like
GRMZM2G136146	PDS5 homolog
Regulatory	
GRMZM2G129444	Mitotic checkpoint protein
GRMZM2G097821	3-phosphoinositide-dependent protein kinase 1
GRMZM2G110922	Serine/threonine-protein kinase SAPK4
GRMZM2G074262	Serine/threonine kinase Nek6-like

Figure 8, Murphy and Bass